Progress in DC Testing of Generator Stator Windings: Theoretical Considerations and Laboratory Tests

Eric David, *Member, IEEE*, and Laurent Lamarre

***Abstract*—The aging due to mechanical, thermal, electrical, and environmental stresses of a stator insulation system inherently involves alterations of the material properties that are detrimental to its service operation. When these properties are deteriorated to the point where the material can no longer operate safely under normal stress conditions, it implies that it has reached the end of its useful life. To prevent such forced outages and improve the useful life, condition-based maintenance and diagnostic tests are periodically conducted on stator insulation systems. Among the tests performed to assess the condition of winding insulation, various methods are commonly used, such as partial discharge measurements, hipot, step voltage, and ramped voltage tests (RTs), to name just a few. DC testing, where the current is continuously monitored, whether during a step voltage test, such as the polarization/depolarization test, or during a linearly increasing voltage test, such as the RT, is commonly used in the field in order to assess the quality of stator winding insulating systems of large synchronous rotating machines. Both of these tests are related to the dielectric response of the insulation system. This paper presents theoretical considerations on the dielectric response of the various types of machine winding insulation systems encounter in the field as well as laboratory results on individual bars and coils.**

***Index Terms*—Dielectric response, machine insulation, polarization and depolarization currents, ramped voltage test (RT).**

I. Introduction

FOR large rotating machines, the search for a practical and reliable diagnostic method to assess the condition of the machine stator insulation system has been ongoing for decades. In order to gain assurance that the winding insulation can safely withstand the service voltage and assess its reliability in operating conditions after a given number of years in service, dc tests have been used for decades [1], [2]. Two common procedures to apply the dc voltage are used in field: the step voltage test, or the polarization/depolarization current test (PDC), and the ramped voltage test (RT), where the voltage is linearly raised up to a predetermined level. In both cases, the current can be continuously recorded. Accordingly, not only some specific quantities, such as the 1-min insulation resistance, but also the material dielectric response in the low-frequency range, from 10^{-1} Hz and below, can be extracted from both techniques with an appropriate modeling. In order to use the occurrence of changes in this low-frequency dielectric response for diagnostic purposes, it is needed to previously completely characterize the dielectric response of the unaged specimen (or one that is in a satisfactory condition) as a function of temperature and voltage level.

The use of dc methods to diagnose the insulation system of large rotating machines is a project that has been going on for more than a decade at the authors' affiliation. The various results and findings from this project have been reported several times [3]–[13], but this is the first time that the complete picture is presented. This paper presents the theoretical background allowing relating the machine insulation dielectric properties to the results of dc testing and the dielectric characterization of the various machine insulation systems. Dielectric response of artificially, laboratory, and field-aged insulation bars, coils, and complete windings will be presented in a subsequent paper.

Manuscript received June 3, 2008; revised January 11, 2009. First published December 22, 2009; current version published February 17, 2010. Paper no. TEC-00202-2008.

E. David is with the Department of Mechanical Engineering, École de technologie supérieure, Montreal, QC H3C 1K3, Canada.

L. Lamarre is with the Hydro-Québec Research Institute (IREQ), Varennes, QC J3X1S1, Canada.

Color versions of one or more of the figures in this paper are available online at http://ieeexplore.ieee.org.

Digital Object Identifier 10.1109/TEC.2009.2025410

II. Theoretical Considerations

A. Basic Relations

The theoretical background related to time-domain dielectric measurements was presented previously [13], [14] and can also be found in the general literature [15]; therefore, we will merely restate the basic equations. In the time domain, the behavior of a linear insulating system is characterized by its conductivity and dielectric response function. When a linear dielectric system between two electrodes is subjected to an arbitrarily time-varying potential difference $U(t)$, the current measured by an external circuit, $I(t)$, is given by

$$I(t) = \frac{C_o \sigma U(t)}{\varepsilon_o} + C_o \frac{\partial}{\partial t}\left[\varepsilon_\infty U(t) + \int_0^\infty f_s(\tau) U(t-\tau) d\tau\right] \tag{1}$$

where $f_s(t)$ is the material dielectric response in the relevant time scale, σ is the effective conductivity of the insulation system (could be a combination of surface and bulk conductivity), ε_∞ is the "infinite-frequency" permittivity, and C_o is the vacuum capacitance. The Laplace transform of (1) yields

$$I(s) = \frac{U(s)}{R_L} + s\left(C_\infty + C_o F(s)\right) U(s) \tag{2}$$

where R_L is the leakage resistance related to the direct conduction current. It is worth mentioning that this resistance is not equivalent to the insulation resistance, as defined by the IEEE Std 43 [2]. The latter is calculated from the total measured current 1 min after the application of the step voltage, and accordingly, includes both the absorption and the conduction contribution (the capacitive surge is usually negligible 1 min after the voltage has reached its steady-state level). The variable $F(s)$ in (2) is the Laplace transform of the dielectric response function.

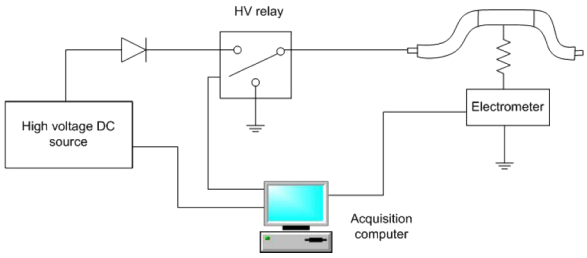

Fig. 1. High-voltage time-domain setup for laboratory measurements.

In order to avoid current fluctuation between the high-voltage source (a switching-type power supply is normally used as voltage source) and the capacitive sample, a measuring resistance is normally placed in series with the sample under test, as shown in Fig. 1. For the case of step voltage test in the field as well as in the laboratory, the measuring resistance is usually small (yielding a time constant less than 0.1 s). However, for the case of an RT on a machine winding in the field, good results are obtained when the value of the resistance in series is chosen in order to obtain a time constant of a few seconds. Accordingly, the presence of such a large resistance in series (in the megohms range) cannot be neglected in the modeling. The voltage drop across the insulation system, $U(s)$ in (2), is then related to the applied voltage function in the Laplacian domain, $E(s)$, by

$$U(s) = E(s) - R_s I(s) \tag{3}$$

where R_s is the instrumental resistance in series with the dielectric under test. By substituting (3) into (2), one obtains

$$I(s) = \frac{E(s)}{R_s + (1/R_L + sC(s))^{-1}} \tag{4}$$

where $C(s)$ is a Laplacian universal capacitance given by

$$C(s) = C_\infty + C_o F(s). \tag{5}$$

Equation (4) can also be written as

$$I(s) = \frac{E(s)\left[1/R_L + sC(s)\right]}{1 + sR_s C(s)} \tag{6}$$

with the assumption that the serial resistance is much lower than the leakage resistance, i.e., $R_s/R_L \ll 1$, which is quite reasonable.

B. Case of a Step Voltage Function

When step voltage tests are used, it normally means that the high-voltage dc power supply is ordered to reach a predetermined voltage level as fast as possible. Then, after a certain charging time t_c, the sample under test is short-circuited usually using a high-voltage relay. This type of test is often identified as the PDC measurement. The mathematical expressions for a true step voltage followed by an instantaneous short circuit are given by the following functions:

$$E(t) = \begin{cases} 0, & t < 0 \\ U_o, & 0 \le t \le t_c \\ 0, & t > t_c \end{cases}$$

$$E(s) = U_o\left[1 - e^{-t_c s}\right]. \tag{7}$$

In order to reach a practical result when combining (6) and (7), some approximations must be used. When assuming that the resistance in series has a significant impact only for the times in the order of the time constant $R_s C_\infty$, one obtains

$$I(t) = \begin{cases} \dfrac{U_o}{R_L} + \dfrac{U_o}{R_s} e^{-t/\tau} + U_o C_o f_s(t), & 0 \le t \le t_c \\ -\dfrac{U_o}{R_s} e^{-(t-t_c)/\tau} - U_o C_o\left[f_s(t-t_c) - f_s(t)\right], & t > t_c. \end{cases} \tag{8}$$

The physical meaning of the three terms in (8), in order of appearance, are, respectively, the direct conduction current (including surface leakage and bulk conductivity), the capacitive current, and the absorption or dielectric relaxation current. The last term of the second equation in (8), the so-called memory term, vanishes for an infinite charging time (assuming a monotonically decreasing response function). In the more realistic case of a finite charging time, a numerical correction can be used to take the finite charging time into account and obtain the real discharge current. This numerical correction procedure, which allows the extraction of the physical meaningful dielectric response function in the previous relation for the discharge current, is surprisingly not a trivial operation. One possible approach is simply to use a very long charging time as compared to the discharge acquisition time (ten times longer charging than discharging is recommended in [15] so that the last term of the right-hand side of the second equation of (8) becomes negligible). Another possibility, when it is not convenient to use a very long charging time, or simply to save measurement time, is to use compensating techniques taking into account the finite charging time [12], [16]. The compensation technique used in this paper assumes that the dielectric response function follows a power law dependency and calculates the parameters of the power law, with the discharge current between 10 and 100 s for a charging time of 1000 s. Then, the compensated discharge current is calculated from (8).

Due to the limited power of a power supply, in reality, a true step voltage function, such as the one given by (7), cannot be applied by the voltage source. Instead, the voltage is roughly linearly raised with a certain rise time t_r up to the desire voltage function. However, usually the rise time is much shorter than the time scale of interest; therefore, it does not significantly alter (8) [17].

C. Case of a Ramped Voltage Function

The dc RT is variation of a dc hipot during which the voltage is ramped up (usually at a low rate in the order of 1 kV/min) and the current is continuously recorded as a function of voltage (or time) [1], [18], [19]. The I–V curve can be plotted in real time, and consequently, if a sudden increase of the recorded current appears in the curve, the test can be interrupted avoiding a possible breakdown. This test not only can serve as a dc withstand test, but can also be used as a diagnostic test with an appropriate analysis of the I–V curve. For a dc high-voltage RT, the Laplace transform of the applied voltage function is given by

$$E(s) = L(\alpha t) = \frac{\alpha}{s^2} \tag{9}$$

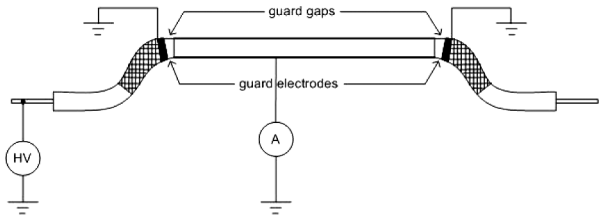

Fig. 2. Electrode configuration for guarded measurements of the straight portion of a bar.

where α is the rate of voltage rise. Substituting (9) into (6) yields

$$I(t) = L^{-1}\left\{\frac{\alpha\left[1/R_L + sC(s)\right]}{s^2\left[1 + sR_sC(s)\right]}\right\}. \tag{10}$$

There is no analytical solution of (10) that allows extraction of the dielectric response function. Using a step voltage test allows a direct evaluation of the three components of the experimental current. This cannot be done with the RT without a prior estimation of the dielectric response function allowing to numerically solve (10).

III. Results and Discussion

A. Measuring System

Charge and discharge currents measured in the laboratory on individual bars were conducted using a two-active-electrode system, consisting of a computer-controlled high-voltage dc source, an electrometer, and high-voltage relay, as illustrated in Fig. 1. To isolate the straight portion of the bar, guarded measurements were conducted with small semiconductive coating rings removed on both sides of the straight portions, as depicted in Fig. 2. This setup is similar to the one described in [20] for guarded measurements. Some measurements were also conducted only with collar guards at the beginning of stress grading layer without disconnecting the semiconductor coating. This technique lowers the contribution of the end-winding portions without suppressing it completely, as is the case when using the arrangement shown in Fig. 2.

B. Low-Frequency Dielectric Response of Unaged Machine Winding Insulation

1) Slot Portion: For machine winding insulation, the absorption current of the straight portion can be assumed to behave approximately in accordance with a universal power law given by

$$I_{\rm abs}(t) = CU_oKt^{-n} \tag{11}$$

where K and n are parameters related to the insulating material, U_o is the magnitude of the voltage step, and C is the capacitance. The aforementioned equation holds for the various machine insulation technologies in the 1–1000 s time range (or 10^{-4} to 10^{-1} Hz frequency range) at room temperature. At higher temperatures, a relaxation peak related to the alpha relaxation of the resin will start to appear, resulting in a change of the dielectric response [10] and (11) will no longer be valid. Accordingly, the dielectric response given by (11) at room temperature can be interpreted as the high-frequency tail of the alpha relaxation peak related to the glass transition temperature.

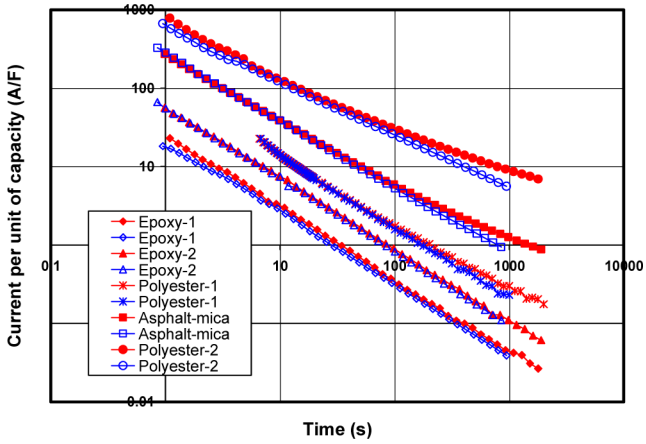

Fig. 3. Normalized charge (filled symbols) and discharge currents (open symbols) for different winding insulation systems after a voltage step of 5 kV: guarded electrode configuration.

Fig. 3 shows the charge and the discharge currents obtained on spare coils insulated with three different insulation technologies: asphalt–mica, early polyester from the mid-1960s (labeled polyester-2); modern polyester (labeled polyester-1); and spare bars insulated with two different epoxy–mica insulation systems (labeled epoxy-1 and epoxy-2). These measurements were conducted at room temperature using the guarded arrangement shown in Fig. 2, and accordingly, reflect only the dielectric response of the straight portions of the bars or coils. The currents are expressed in per unit of capacitance, and accordingly, are called normalized currents later in the text.

One can see that (11) gives a reasonable fit to the experimental data for all technologies shown in Fig. 3. Indeed, according to (8), the absorption current is given by discharge current once the capacitive surge has vanished. The dielectric response function is then related to the parameters in (11) by

$$f(t) = At^{-n} = K\frac{C}{C_o}t^{-n}. \tag{12}$$

Fitting power laws to the discharge currents yielded the parameters shown in Table I. More than one order of magnitude in the absorption current can be observed for the different technologies. It can also be seen in Fig. 3 that the modern insulation system using epoxy and polyester resin as bonding agent are characterized by very low bulk conductivity, while older technology, early polyester and asphalt insulation systems, are naturally slightly conductive. All the parameters shown in Table I were calculated from charge and discharge curves at 5 kV. The *RC* and *RC′* parameters in Table I are, respectively, the ratio of the applied voltage and the normalized charge and discharge current at 60 s. These parameters can be related to the dissipation factor at $1/600$ Hz using the Hamon approximation [21]

$$\tan\delta\,(0.00167\ \text{Hz}) = \frac{300}{\pi RC}. \tag{13}$$

The dissipation factor related to the *RC* parameter includes the losses due to leakage and absorption currents, while the one

TABLE I
DIELECTRIC PARAMETERS FOR THE MEASUREMENTS SHOWN IN FIG. 3

	K $s^{(n-1)}$	n	PI	RC at 60 s (s)	RC' at 60 s (s)
Epoxy-1	0.0041	0.91	8.0	8710	9970
Epoxy-2	0.012	0.93	8.4	3550	3750
Polyester-1	0.021	0.90	6.2	1800	1870
Polyester-2	0.12	0.68	3.6	121	140
Asphalt	0.054	0.85	5.2	565	615

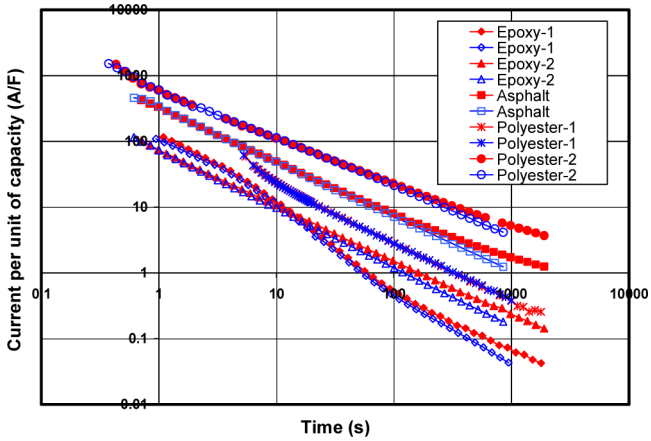

Fig. 4. Normalized charge (filled symbols) and discharge currents (open symbols) for different winding insulation systems after a voltage step of 5 kV: unguarded electrode configuration.

related to the RC' includes the losses only due to the absorption current, whether coming from dipolar or interfacial polarization mechanisms. As we can see in Table I, these parameters depend tremendously upon the chemical nature of the insulation components. More than an order of magnitude in the dielectric loss can be observed for the different bonding resins.

2) Complete Bars/Coils: When unguarded measurements are conducted on a complete bar or on a complete winding in the field, the dielectric response due to the end-winding portions superimposes to the one from the straight sections. Unguarded measurements on the complete bars were also conducted using the experimental setup illustrated in Fig. 1. The normalized charge and discharge currents for the five samples are shown in Fig. 4. The stress grading system of the epoxy-1 bar was a SiC-based stress grading coating, while it was a ferrous-oxide-based stress grading paint for both the epoxy-2 bar and the polyester-1 coil. Iron oxide stress grading paints are rarely used nowadays, but a large number of machines in service still use this type of stress control system. For the asphalt and polyester-2 coil, the absorption current from the straight section is high enough that the dielectric response related to the stress grading system has only a negligible contribution to the total measured currents. A complication that arises for the insulating system labeled epoxy-1, as can be seen in Fig. 4, is the occurrence of a relaxation peak when unguarded measurements were used. This peak is related to an interfacial polarization mechanism between the SiC-based stress grading coating and the insulation wedge. Further discussion on this subject can be found elsewhere [7], [12]. The same parameters that were calculated for the guarded measurements were also calculated for the complete bars and coils, and are shown in Table II. The RC' parameter is a very relevant parameter that can be used for comparison with field measurement on complete windings since it is independent of the sample size (or the number of bars/coils). However, it is strongly dependent upon the nature of the insulation system, the temperature, and, to a lesser extent, upon the magnitude of the applied voltage. Accordingly, it must be corrected to a common temperature with an appropriate correction factor. When temperature is taken into account, the RC' parameter can be used to trend the condition of the bonding resin [3], [5], [12], [14], [22]. An abnormally low value of this parameter, which translates a high value of absorption current, normally reflects a lack of curing, thermal aging, or moisture absorption in the bulk. Obviously, to point out what is an abnormally high absorption current, the expected magnitudes of the absorption current of the various insulation technologies in a satisfactory condition need to be known, since order of magnitude in the value of both normalized resistances, RC and RC', can be found between the different unaged winding insulation technologies. This concept is somewhat taken into account in the IEEE Std 43, with the recommendation of two different thresholds for the minimum insulation resistance value for windings made before 1970 (asphalt and polyester-2 insulation systems) and after 1970 (epoxy-1, epoxy-2, and polyester-1 insulation systems).

TABLE II
DIELECTRIC PARAMETERS FOR THE MEASUREMENTS SHOWN IN FIG. 4

	K $s^{(n-1)}$	n	PI	RC at 60 s (s)	RC' at 60 s (s)
Epoxy-1	-	-	10	4970	5780
Epoxy-2	0.015	0.89	6.5	2160	2670
Polyester-1	0.033	0.88	7.4	1080	1090
Polyester-2	0.13	0.74	4.9	149	157
Asphalt	0.065	0.83	5.1	462	466

Due to the interfacial polarization mechanism that takes place at the stress grading paint and the insulation material interface, the absorption current for the epoxy-1 bar does not fit a power law behavior anymore, and therefore, no K and n parameters could be calculated. Also, the relatively high value of the PI translates the deformation of the charge and discharge curves due to the polarization mechanism.

3) Modern Epoxy–Mica Insulation System: Modern epoxy–mica insulation systems, such as the insulation systems labeled epoxy-1 and epoxy-2, are characterized by particularly low dissipation factor, and accordingly, both RC and RC' parameters should be above 2000 s when measured at room temperature [23]. However, in some cases, the stress grading system has a dominating influence on the normalized resistance values. It results in much lower normalized resistance values than what would be expected. Fig. 5 shows PDC measurements for voltage levels from 1 to 20 kV for two similar modern epoxy–mica bars, one with iron oxide stress grading paint [Fig. 5(a)] and the other one with SiC tape added on the stress grading paint [Fig. 5(b)]. One can see that the type of stress grading system has a large impact on both the shape and the magnitude of the polarization and depolarization currents for modern epoxy–mica insulated

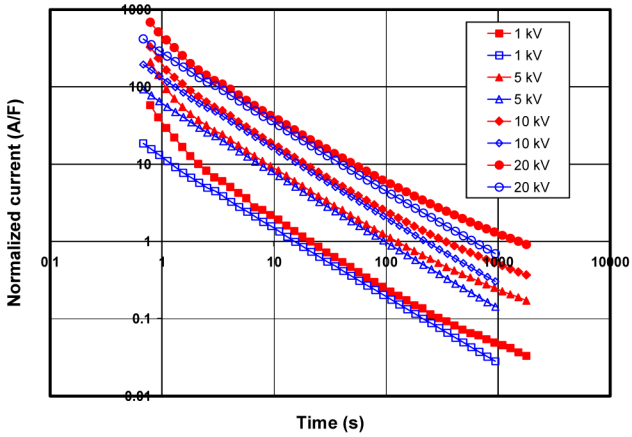

(a)

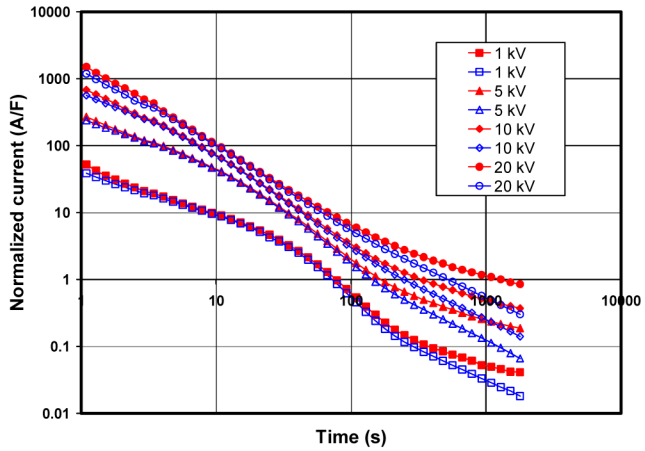

(b)

Fig. 5. Normalized charge (filled symbols) and discharge currents (open symbols) for the same epoxy–mica bar with (a) ferrous oxide stress grading system and (b) SiC tape added on the ferrous oxide paint.

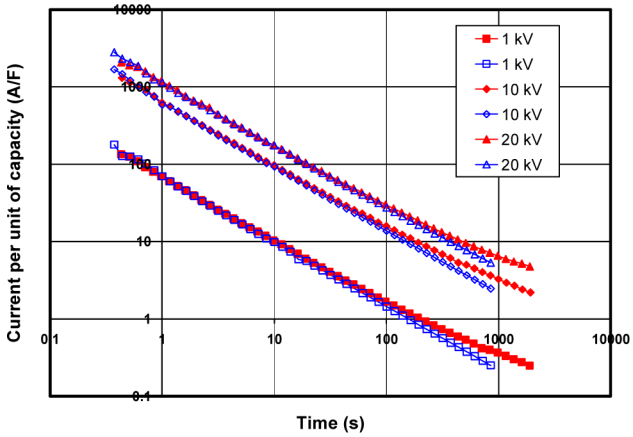

(a)

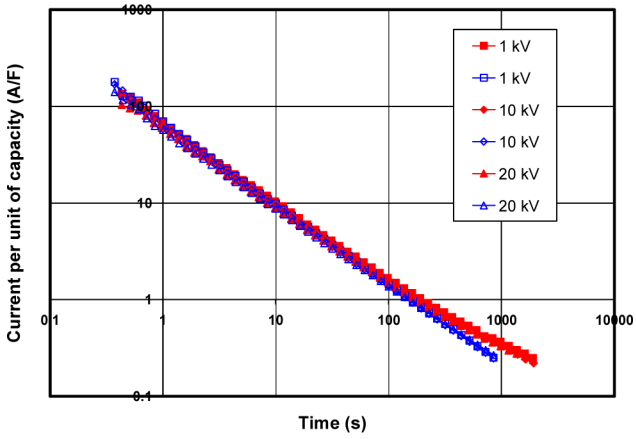

(b)

Fig. 6. Time-domain measurements on an unaged asphalt–mica coil: (a) charge (filled symbols) and discharge (open symbols) currents at 1, 10, and 20 kV; (b) charge and discharge currents corrected to 1 kV.

TABLE III
DIELECTRIC PARAMETERS FOR THE MEASUREMENTS SHOWN IN FIG. 5 AT 5 KV AND FOR THE SAME MEASUREMENTS WITH A GUARDED ELECTRODE

	PI	RC	RC'	RC' guarded
No SiC tape	5.6	3420	4090	4750
SiC tape	13	1120	1210	3900

windings (Table III). Indeed, the resistance for the bar with the SiC tape was three times lower than for a similar bar with only the ferrous oxide paint as stress grading system. Also, the polarization index was strongly affected by the type of stress grading system, yielding much higher value than expected for the bar with the SiC tape.

Guarded measurements were also conducted on the same bars, but without introducing a gap in the semiconductive slot coating, which results in a less efficient separation of the end-winding contribution. Nevertheless, a three-time increase in resistance was measured for the bar with the SiC tape when guarded measurements were used.

4) Linearity: The validity of (6) is somewhat based upon the supposition that the insulation system behaves linearly. Figs. 6–8 show the normalized charge and discharge currents for an asphalt–mica coil and the epoxy–mica-2 and epoxy–mica-1 bars, respectively, after step voltages of 1, 10, and 20 kV. Figs. 6(b), 7(b), and 8(b) depict the same curves but corrected to 1 kV, which means that the 10 kV curves are divided by 10 and the 20 kV curves are divided by 20. In the case of a linear dielectric system, the current traces would then all superimpose. As can be seen in Fig. 6, the asphalt–mica insulating system behaves linearly, with respect to both the absorption and the conduction currents, up to 20 kV. However, the epoxy–mica insulation system shows some nonlinearity, which is expressed by the nonsuperimposition of the curves when corrected to 1 kV. This is caused by the stress grading system, and the magnitude of the nonlinearity strongly depends on the design of the stress grading system. The iron oxide paint, which forms a more capacitive type of stress grading system, is less conductive, and accordingly, does not lead to a sharp interfacial peak. This is shown in Fig. 7. SiC-based stress grading systems, either paint or tapes, are more conductive than iron oxide systems, and their conductivity is strongly nonlinear under ac or dc voltage. This is shown in Fig. 8, where one can clearly see an interfacial relation peak decreasing in magnitude and moving toward shorter times as the voltage increases. The nonlinear contribution from the

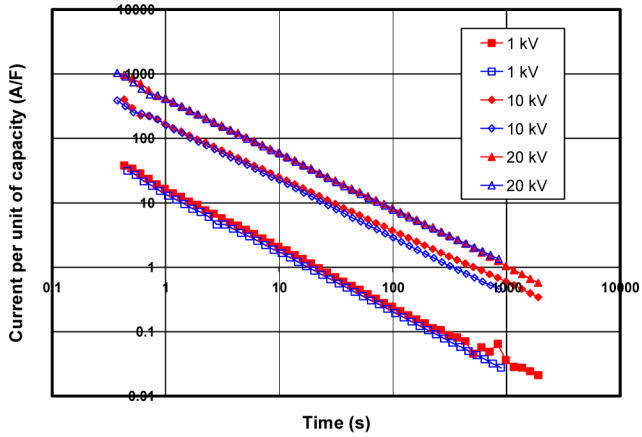

(a)

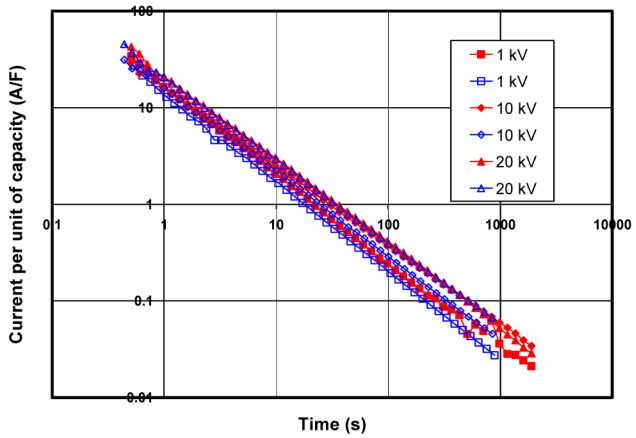

(b)

Fig. 7. Time-domain measurement on an unaged epoxy–mica bar with ferrous oxide stress grading paint: (a) charge (filled symbols) and discharge (open symbols) currents at 1, 10, and 20 kV; (b) charge and discharge currents corrected to 1 kV.

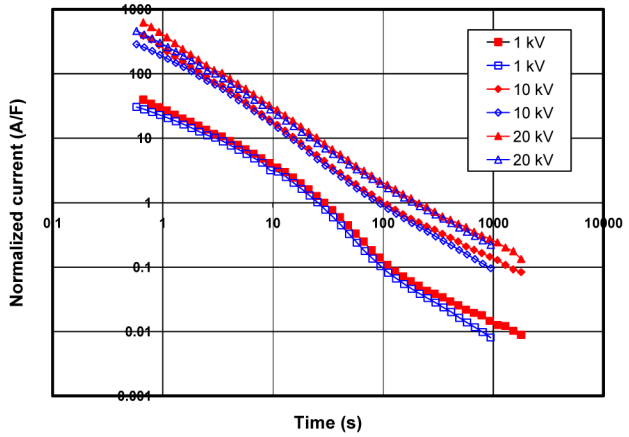

(a)

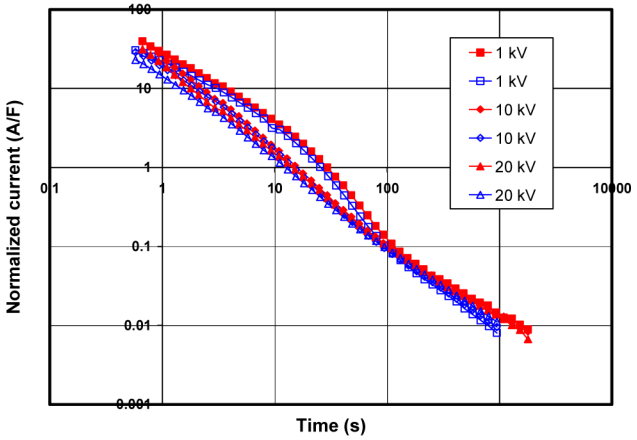

(b)

Fig. 8. Time-domain measurement on an unaged epoxy–mica bar with SiC stress grading system: (a) charge (filled symbols) and discharge (open symbols) currents at 1, 10, and 20 kV; (b) charge and discharge currents corrected to 1 kV.

stress grading system cannot be seen for the asphalt–mica coil (a graphite-based stress grading system) since the magnitude of the absorption current per unit of capacitance from the straight portion, which is linear, is much greater than for epoxy–mica insulating systems and dominates the total dielectric response.

Another way to point out the occurrence of nonlinearity is to convert the time-domain currents into the frequency domain, which has the natural consequence of normalizing the current traces by the voltage magnitude. Fig. 9 shows the dielectric response for a modern epoxy–mica insulated bar with SiC-based tape used as stress grading systems. The charge currents after voltage steps of 1–20 kV were normalized to the bar capacitance and converted into the frequency domain by using the Hamon approximation [21]. The nonlinearity of the stress grading system can be clearly seen in Fig. 8(a), while the dielectric response of the insulation system in the slot portion remains almost perfectly linear up to 20 kV.

Being able to recognize nonlinear relaxation peaks due to the stress grading system is particularly valuable since insufficient curing can also lead to a relaxation peak within the same frequency range. This is later related to a dipolar polarization mechanism rather than an interfacial polarization mechanism. In this case, there is no change in the peak magnitude or frequency with voltage. Fig. 10 shows the results of a PDC test on the straight section of a modern epoxy–mica bar that was discarded from a lot of bars [23] used to rewind a 150-MVA hydrogenerator due to a suspected lack of curing. Higher dielectric loss and a small relaxation peak in the 10^{-3} to 10^{-2} Hz frequency range can be observed. As can be seen, contrary to the peak related to the stress grading system, this peak remains perfectly linear with respect to the applied voltage.

5) Temperature: In order to make a meaningful comparison for field (or laboratory) measurements conducted at different temperatures, the influence of temperature on the dielectric properties of machine insulation systems must be taken into account. Accordingly, it is recommended in the IEEE Std 43 [2] to correct all insulation test values to a common base temperature of 40 °C. The correction may be made using the following equation:

$$R_c = K_T R_T \tag{14}$$

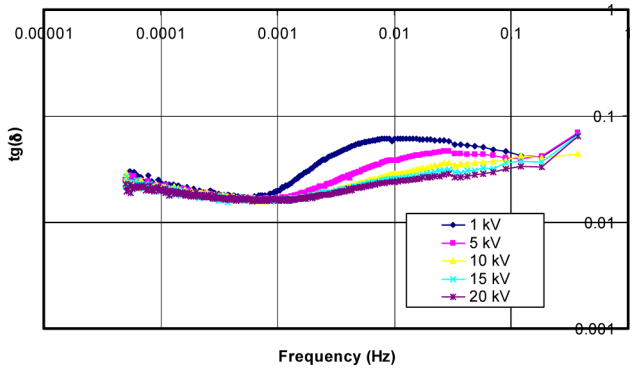

(a)

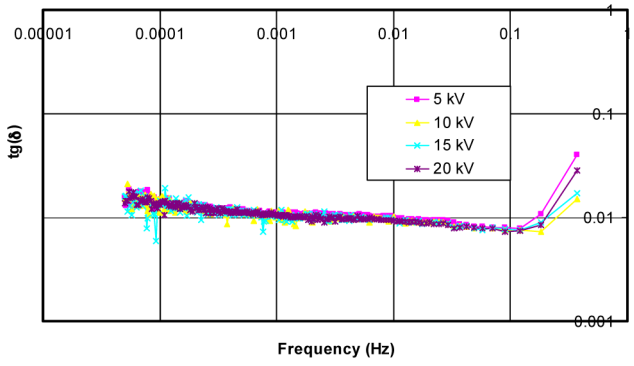

(b)

Fig. 9. Charge currents from 1 to 20 kV for a modern epoxy–mica bar converted into the frequency domain: (a) complete bar and (b) straight portion.

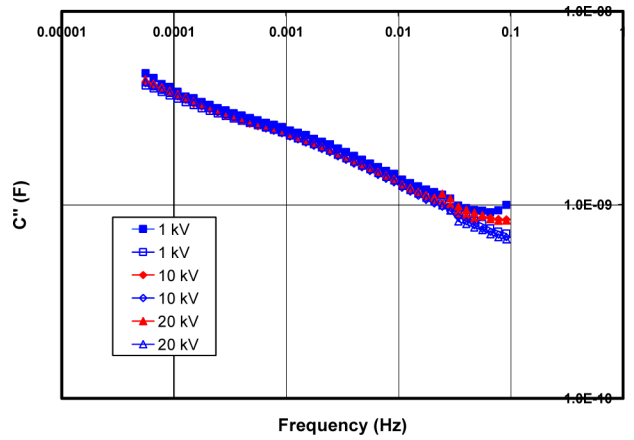

Fig. 10. Charge and discharge currents from 1 to 20 kV for a modern epoxy–mica bar with incomplete curing. The currents were converted into the frequency domain with the help of the Hamon approximation.

where R_c is the insulation resistance corrected at 40 °C, K_T is the correction factor at temperature T, and R_T is the insulation resistance as measured at temperature T. The influence of temperature on the dielectric response of a machine insulation system has recently been the subject of several reports [10], [14], [24]–[26], mostly aiming to provide more reliable equations for the insulation resistance correction factor than what is suggested in the standard 43. Indeed, it has been shown from laboratory measurements on bars and coils that

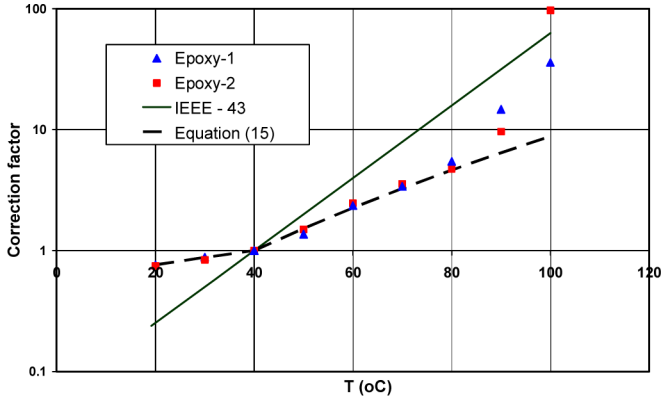

Fig. 11. Comparison between the experimental results for the two epoxy–mica insulation systems and the proposed model [see (15)].

TABLE IV
PARAMETERS FOR THE TEMPERATURE CORRECTION THAT APPLIES TO MODERN BAR INSULATIONS (NEW PROCEDURE)

Temperature Range	B (K)
20°C < T < 40°C	1245
40°C < T < 85°C	4230

the variation of the insulation resistance for modern thermosetting insulation systems is much lower than what is predicted by IEEE Std 43. In other words, it means that an insulation resistance measurement conducted at 20 °C and corrected to 40 °C by the procedure in the standard would have a much lower resistance than the actual measurement conducted at 40 °C.

Fig. 11 shows the results of insulation resistance measurements for epoxy-1 and epoxy-2 for temperature from 20 °C to 100 °C [26]. It can be seen that the IEEE-suggested equation for K_T does not fit the experimental data. The equation

$$K_T(T) = \exp\left[-B\left(\frac{1}{T} - \frac{1}{T_o}\right)\right] \tag{15}$$

was found to give a very good fit for the experimental results for 20 °C $< T <$ 85 °C, with the coefficient B given by the values in Table IV. Both T and T_o in (15) are in Kelvin, with $T_o = 313$ K.

A detailed analysis of the data illustrated in Fig. 11 is given elsewhere [26].

C. DC Ramped Voltage

DC RT was conducted on bars and coils using the same experimental setup as for the PDC test (see Fig. 1). The applied voltage was smoothly raised at the rate of 1 kV/min up to 25 kV, while the current was continuously monitored. To avoid current fluctuations due to the digitalized ramp, the resistor added in series was chosen in order to increase the instrumental time constant to the 10 s range. In order to separate the contributions of the leakage, and the absorption and the capacitive currents to the total current, (10) must be solved. Substituting (5) and (12) into (10) yields

$$I(t) = L^{-1}\left\{\frac{\alpha\left[1/R_L + sC_\infty + Bs^n\right]}{s^2\left[1 + R_s\left(sC_\infty + Bs^n\right)\right]}\right\} \tag{16}$$

where B is given by

$$B = KC_\infty \Gamma(1-n). \tag{17}$$

Equation (16) can then be solved numerically by a line integration in the complex plane. Several algorithms are available in the literature [26]. The unknown parameters K, n, and R_L can then be adjusted to give the best fit to the experimental curve. More details on the procedure are given elsewhere [13]. Alternatively, an approximate solution of (16) can be obtained by neglecting the power law term in the denominator. The analytical solution of (16) then becomes

$$I(t) = \frac{\alpha}{R_L}\left[t - \tau\left(1 - e^{-t/\tau}\right)\right] + \alpha C_\infty \left(1 - e^{-t/\tau}\right) + I_{\rm abs}(t) \tag{18}$$

$$I_{\rm abs}(t) = \frac{\alpha B}{\Gamma(2-n)} t^{1-n} - \frac{\alpha B}{\Gamma(1-n)} \int_0^t e^{-(t-x)/x} x^{-n}\, dx \tag{19}$$

with $\tau = R_s C_\infty$. These equations will be referred to as the approximate linear model, since a linear dielectric behavior (σ and $f(t)$ independent of the magnitude of the electric field) was assumed in their development. Thus, if any nonlinearity occurs in the experimental curve, a deviation will be seen between the experimental data and the linear model. The first two terms of (18) are, respectively, the direct conduction (or leakage) and the capacitive currents. The term $(1 - e^{-t/\tau})$ is responsible for the slightly rounded current response at the beginning of the I–V curves, as shown in Fig. 9. The absorption current is given by (19). The second term in (19) can be readily evaluated by numerical methods. However, it is usually small compared with the first term, and approximating the absorption current using only the first term of (19) often yields reasonably good fits with the experimental results.

The experimental current traces for the asphalt–mica coil and the epoxy–mica-1 bar are, respectively, shown in Fig. 12(a) and (b). The dashed line represents the contribution of both the absorption and capacitive current according to the model. Consequently, by subtracting this line from the experimental data, one obtains the contribution of the leakage current. The contribution of the capacitive current alone is also plotted and represented by the dotted–dashed line so that the magnitude of the absorption current, which is given by the difference between the two dashed curves, can be visualized. As expected, the absorption current was found to be much higher for the asphalt–mica technology than for the epoxy–mica technology.

The parameters yielding the best fit for both models are listed in Table V. The approximate linear model was found to give a very good agreement with the experimental data. The extracted parameters in Table V were also found to be in good agreement with the same parameters measured by PDC tests. The nonlinearity originating from the stress grading system for the epoxy bar could not be observed using the RT. For both insulation systems, unaged clean and dry, the dielectric response was found to be linear up to 25 kV (no deviation from the linear solutions). The leakage current for the epoxy–mica system was found to be higher than the value obtained from step voltage test, but this

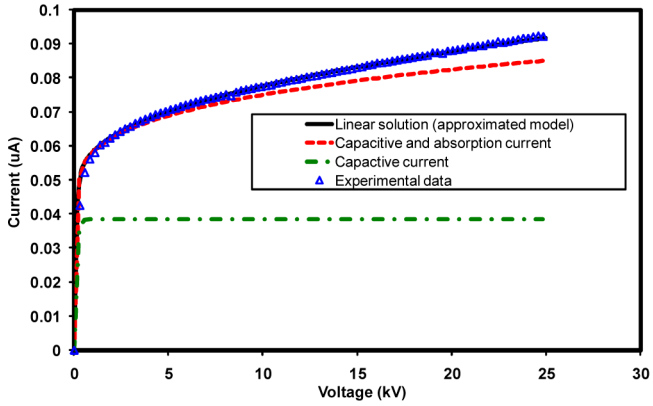

(a)

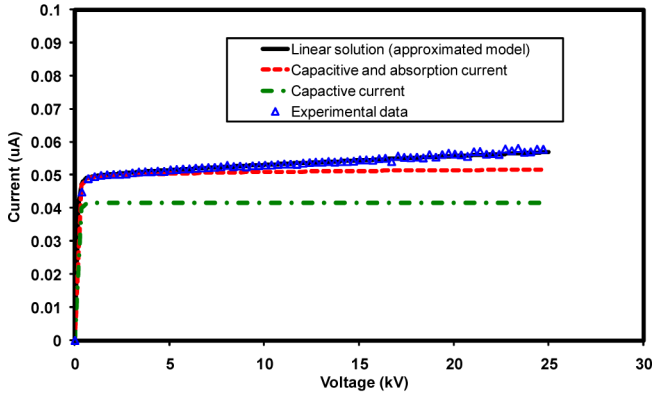

(b)

Fig. 12. Comparison between experimental measurements and the approximate model for (a) asphalt–mica spare coil and (b) epoxy–mica spare bar. The dashed curve is the contribution of both the capacitive and absorption currents, while the dotted–dashed curve is the contribution of the capacitive current alone.

TABLE V
DIELECTRIC PARAMETERS EXTRACTED FROM THE FITTING OF THE EXPERIMENTAL DATA

	K $s^{(n-1)}$	n
Epoxy-2	0.011	0.92
Asphalt	0.046	0.74

value for unguarded measurement on low-conductivity insulation material can vary significantly due to small change in the environmental conditions from one measurement to the other.

Fig. 13 shows the I–V curve from a ramp voltage test conducted on the polyester-1 coil. The point at which the experimental I–V curve deviates from the linear model (approximately 22 kV, as can be seen in Fig. 13) defines the onset of the nonlinearity. At this voltage, the leakage current starts to increase abnormally. Leakage current values can then be calculated by subtracting the experimental current from the calculated absorption and capacitive currents. This procedure assumes that the deviation from the linearity originates from a nonlinear increase of the leakage current while the absorption current remains linear. The onset of nonlinearity is related to the degree of aging of the insulation system. Thus, trending measurements done on a similar ma-

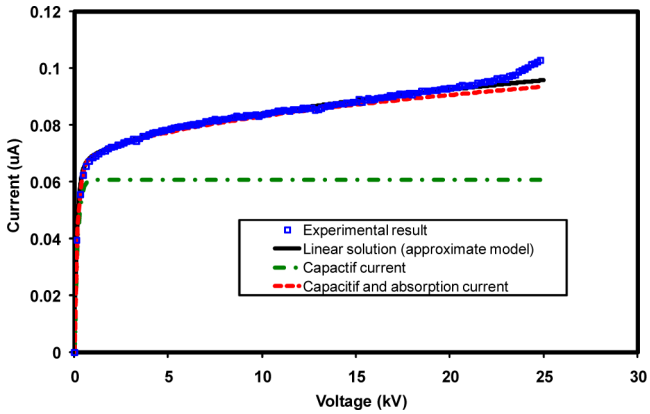

Fig. 13. Comparison between experimental measurements and the approximate model for the polyester-1 spare coil. The dashed curve is the contribution of both the capacitive and absorption currents, while the dotted–dashed curve is the contribution of the capacitive current alone.

chine at regular intervals of time could lead to an estimation of the rate of aging.

IV. Conclusion

Modern equipment allows conducting automated dc testing of machine insulation. With a computer-controlled high-voltage dc source, any arbitrary voltage function can be applied on the insulation system. The common voltage functions used include the step voltage function, leading to the measurement of polarization and depolarization currents, and the linearly increasing voltage function, known as the RT. In both cases, the dielectric equations can be solved, thus yielding the three components of the measured current, which are the absorption, leakage, and capacitive currents. The peculiarities of the insulation system can then be precisely pointed out. This includes the magnitude of the dielectric loss (or absorption) current, the presence of excessive leakage, the specific contribution of the various types of stress grading systems, and the onset of nonlinearity in the absorption and leakage currents. The magnitude of the absorption current varies considerably with different winding technologies; therefore, one must be careful when using only this parameter as a diagnostic parameter to detect degradation of the bonding resin. Also, the presence of SiC-based stress grading tapes will usually lead to a large relaxation peak, especially at test voltages below 5 kV, leading to a considerable decrease of the insulation resistance, which has nothing to do with the quality of the insulation system.

The RT, although less precise than PDC tests for the determination of the dielectric properties of the insulation system, can give a good estimation of the dielectric parameters in a relatively short testing time. It is not much affected by the natural nonlinearity of the stress relief coatings. Furthermore, it is a very convenient test to precisely point out the onset of nonlinearity in the response of the insulation system. Since the voltage is ramped up at a slow rate, the test can be safely interrupted as soon as the current starts to increase rapidly.

Acknowledgment

The authors gratefully acknowledge the expert technical support of C. Guddemi.

References

[1] *IEEE Recommended Practice for Testing Insulation Testing of AC Electric Machinery (2300 V and Above) With High Direct Voltage,* IEEE Standard 95-2002, 2002.

[2] *IEEE Recommended Practice for Testing Insulation Resistance of Rotating Machinery,* IEEE Standard 43-2000, 2000.

[3] E. David, L. Lamarre, and D. N. Nguyen, "The use of time domain spectroscopy as a diagnostic tool for rotating machine windings," in *Conf. Rec. 2002 Int. Symp. Electr. Insul. (ISEI)*, pp. 506–510.

[4] E. David, R. Taghizad, L. Lamarre, and D. N. Nguyen, "Investigation on the low frequency dielectric response of ground wall insulation of rotating machine windings," in *Proc. 2003 Annu. Rep. Conf. Electr. Insul. Dielectr. Phenom. (CEIDP)*, pp. 157–160.

[5] E. David, L. Lamarre, and D. N. Nguyen, "Low-frequency dielectric response of asphalt bonded insulation," in *Proc. 8th Int. Conf. Conduction Breakdown Solids Dielectr. (ICSD)*, 2004, pp. 497–500.

[6] C. Paynot, L. Lamarre, E. David, and R. Taghizad, "The use of transient current for the evaluation of the condition of rotoric and statoric insulation systems of large synchronous rotating machines," presented at the Electr. Electron. Insul. Conf., EEIC/ICWA Expo., Indianapolis, IN, 2005.

[7] E. David and L. Lamarre, "Modelization of the low-frequency dielectric response of rotating machine stator insulation system," in *Proc. 2005 Annu. Rep. Conf. Electr. Insul. Dielectr. Phenom. (CEIDP)*, pp. 257–260.

[8] C. Paynot, L. Lamarre, E. David, and R. Taghizad, "The use of transient current for the evaluation of the condition of rotoric and statoric insulation systems of large synchronous rotating machines," presented at the 2005 Electr. Insul. Conf. (EIC), Indianapolis, IN, Paper 5-3(43).

[9] G. R. Soltani and E. David, "Condition assessment of rotating machine winding insulation by analysis of charging and discharging currents," in *Proc. 2006 IEEE Int. Symp. Electr. Insul. (ISEI)*, pp. 336–339.

[10] L. Lamarre and E. David, "Dielectric response of rotating machine stator insulation system," in *Proc. 2006 Annu. Rep. Conf. Electr. Insul. Dielectr. Phenom. (CEIDP)*, pp. 549–552.

[11] E. David, A. Nair, T. Godin, and J. Bellemare, "Modeling of a generator I–V curve from the ramped direct voltage method," in *Proc. 2006 IEEE Int. Symp. Electr. Insul. (ISEI)*, Toronto, ON, Canada, pp. 10–13.

[12] E. David and L. Lamarre, "Low-frequency dielectric response of epoxy–mica insulated generator bars during multi-stress aging," *IEEE Trans. Dielectr. Electr. Insul.*, vol. 14, no. 1, pp. 212–226, Feb. 2007.

[13] E. David, T. Godin, J. Bellemare, and L. Lamarre, "Modeling of the dielectric response of a stator winding insulation from a DC ramp test," *IEEE Trans. Dielectrics Electr. Insul.*, vol. 14, no. 6, pp. 1548–1558, Dec. 2007.

[14] M. Farahani, H. Borsi, and E. Gockenbach, "Dielectric response studies on insulation system of high voltage rotating machines," *IEEE Trans. Dielectr. Electr. Insul.*, vol. 13, no. 2, pp. 383–393, Apr. 2006.

[15] A. K. Jonscher, *Dielectric Relaxation in Solids*. London, U.K.: Chelsea Dielectrics Press, 1984.

[16] A. Helgesen, "Analysis of dielectric response measurement methods and dielectric properties of resin-rich insulation during processing," Doctoral dissertation, Roy. Inst. Technol. (KTH), Stockholm, Sweden, 2000 (ISSN 1100-1593).

[17] E. David and L. Lamarre, "Influence of risetime on the dielectric parameters extracted from time domain spectroscopy," *IEEE Trans. Dielectr. Electr. Insul.*, vol. 12, no. 3, pp. 423–428, Jun. 2005.

[18] L. Rux and M. Sasic, "Advantages of the ramped direct high-voltage method of assessing stator winding insulation condition," in *Proc. Hydro-Vision*, 2004, pp. 1–13.

[19] L. Rux and B. Mcdermid, "Assessing the condition of hydrogenerator stator insulation using the ramped high direct-voltage test method," *IEEE Electr. Insul. Mag.*, vol. 17, no. 6, pp. 27–33, Nov./Dec. 2001.

[20] *IEEE Recommended Practice for Measurement of Power Factor Tip-Up of Electric Machinery Stator Coil Insulation,* IEEE Standard 286-2000, 2000.

[21] B. V. Hamon, "An approximate method for deducing dielectric loss factor from direct-current measurements," *Proc. Inst. Electr. Eng.*, vol. 99, pp. 151–155, 1952.

[22] A. Tabarneo, B. Batlle, L. M. Lopez, A. Villaruba, S. Rodriguez, and O. Martinez, "EDA test to perform predictive maintenance in relevant rotating machines," presented at the CIGRE Session 2008, Paris, France.

[23] E. David, L. Lamarre, and D. N. Nguyen, "Measurements of polarization/depolarization currents for modern epoxy–mica bars in different conditions," in *Proc. 28th Electr. Insul. Conf.*, 2007, pp. 202–206.
[24] H. Zhu, "Insulation resistance measurements versus temperature made on aged stator bars and coils," in *Proc. 28th Electr. Insul. Conf.*, 2007, pp. 189–192.
[25] L. Lamarre, D. N. Nguyen, and E. David, "Temperature and voltage dependence of dielectric properties of modern epoxy mica insulations of HV rotating machines," in *Proc. 28th Electr. Insul. Conf.*, 2007, pp. 99–102.
[26] L. Lamarre and E. David, "Temperature dependence of the resistance of modern epoxy mica insulations of HV rotating machines," *IEEE Trans. Dielectr. Electr. Insul.*, vol. 15, no. 5, pp. 1305–1312, Oct. 2008.
[27] F. Veillon, "Numerical inversion of Laplace transform," *Commun. ACM*, vol. 17, pp. 587–590, 1974.

Eric David (M'02) was born in Montreal, QC, Canada, in 1965. He received the M.Sc.A. and Ph.D. degrees in engineering physics from the École Polytechnique de Montréal, Montreal, in 1989 and 1996, respectively.

In 1998, he joined the Hydro-Québec Research Institute (IREQ), where, from 2001 to 2002, he was engaged in the field of dielectric materials used for underground cables and rotating machines. He is currently a Professor in the Department of Mechanical Engineering, École de technologie supérieure, Montreal. His current research interests include dielectric materials, rotating machinery, and underground cable insulation.

Laurent Lamarre was born in St-Jean-sur-Richelieu, QC, Canada, in 1952. He graduated in 1975 in engineering physics from the École Polytechnique de Montréal, Montreal, QC, and received the Master's degree in engineering physics from the École Polytechnique de Montréal in 1978 and the Ph.D. degree in materials science from Massachusetts Institute of Technology (MIT), Cambridge, in 1983.

Since 1983, he has been with the Hydro-Québec Research Institute (IREQ), Varennes, QC, and possesses a 21-year experience in research in electrical apparatus, with the last seven years dealing with rotating machinery insulation.